Kalifersite, a new alkaline silicate from Kola Peninsula (Russia) based on a palygorskite-sepiolite polysomatic series

GIOVANNI FERRARIS *, ALEXANDER P. KHOMYAKOV **, ELENA BELLUSO *
and SVETLANA V. SOBOLEVA ***

* Dip. Scienze Mineralogiche e Petrologiche, Univ. Torino,
Via Valperga Caluso 35, I-10125 Torino, Italy. − e-mail: ferraris@dsmp.unito.it
** Inst. of Mineralogy, Geochemistry and Crystal Chemistry of Rare Elements,
Russian Acad. Sci., Veresaev st. 15, RU-121357 Moscow, Russia
*** Inst. of Ore Deposits, Petrography, Mineralogy and Geochemistry,
Russian Acad. Sci., Staromonetny per. 35, RU-109017 Moscow, Russia

Abstract: Kalifersite, $(K, Na)_5(Fe^{3+})_7[Si_{20}O_{50}](OH)_6 \cdot 12H_2O$, is a new [001] fibrous silicate discovered in a drill core of a hydrothermally altered pegmatite in the urtite series at Mt. Kukisvumchorr (Kola Peninsula). The new mineral formed by crystallization from residual peralkaline liquids during the hydrothermal stage of the pegmatitic process. Pink-brownish; good {100} and {010} cleavages; D$(meas)$ = 2.37(2) g/cm^3. Biaxal (+); α = 1.523(2), β = 1.525(2), γ = 1.550(2), 2V$(meas)$ = 30(2)°, 2V$(calc)$ = 32°; optically pseudo-orthorhombic, O.P. (010); slightly pleochroic. SAED patterns show triclinic symmetry and streaks; a = 14.86(4), b = 20.54(4), c = 5.29(2) Å, α = 95.6(3), β = 92.3(3), γ = 94.4(3)° have been obtained from least-squares refinement of powder diffraction data; s.g. $P\bar{1}$, Z = 1. Comparison with sepiolite {$Mg_8[Si_{12}O_{30}](OH)_4 \cdot 12H_2O$; a = 13.40, b = 26.80, c = 5.28 Å, s.g. $Pncn$, Z = 2} and palygorskite {$Mg_5[Si_8O_{20}](OH)_2 \cdot 8H_2O$; a = 13.27, b = 17.868, c = 5.279 Å, β = 107.38°, s.g. $C2/m$, Z = 2} allowed to obtain for kalifersite a structural model which explains its characteristics. On the basis of $P = [(Y^{2+})_{5-y'-z'}(Y^{3+})_{y'} \square_{z'}][Si_8O_{20}](OH)_2\{(A^{n+})_{(2z'-y')/n} \cdot m'H_2O\}$ (palygorskite module) and $S = [(Y^{2+})_{8-y-z}(Y^{3+})_y \square_z][Si_{12}O_{30}](OH)_4\{(A^{n+})_{(2z-y)/n} \cdot mH_2O\}$ (sepiolite module), kalifersite is the P_1S_1 member (with $y + y'$ = 7, $z + z'$ = 6 and $m + m'$ = 12) of a P_pS_s polysomatic series named *palysepiole series*. In kalifersite, the alkali cations A lie in octahedra which connect the Y-octahedra belonging to the palygorskite/sepiolite framework. This feature and polysomatic aspects are discussed by comparison with biopyriboles, raite and, in general, 2:1 layer silicates.

Key-words: kalifersite, new mineral, polysomatism, palygorskite, sepiolite, raite.

Introduction

The hyperagpaitic rocks with unique geochemistry occurring in the Khibina-Lovosero complex (Kola Peninsula, Russia) are particularly fertile in bearing more than 500 different minerals which include over 100 new species (Khomyakov, 1995). Several of these minerals are characterized by a large alkalis/(other cations) ratio and, particularly silicates, are based on unique structures well suited to lodge large quantities of alkaline cations (*e.g.*, Ferraris *et al.* 1995). Often these silicates show fibrous morphology (Khomyakov, 1995) which usually corresponds to poorly crystallized material and disorder around the fibre axis. That can prevent classical structural studies based on single-crystal diffraction. Fortunately, the structural classification of a large number of silicate structures (*e.g.*, Liebau 1985; Lima-de-Faria, 1994) allows the utilization of recurring structural features, particularly when these have been theoretically rationalized, as in the case of the polysomatic theory (Thompson, 1978). Following similar cases concerning Kola minerals

(Egorov-Tismenko & Sokolova, 1990; Ferraris *et al.*, 1996b, 1997), polysomatism has been the key to characterize the new silicate kalifersite (Ferraris *et al.*, 1996a) and results are presented in this paper.

The name kalifersite is given with reference to chemical composition (*kali*um, *fer*rum, *si*licium). Name and species have been approved by the Commission on New Minerals and Mineral Names of IMA (N° 96–007). Type material is deposited in the Fersman Mineralogical Museum (Moscow, Russia; N° 2234) and Museo Regionale di Storia Naturale (Torino, Italy N° 1998001.01).

Table 1. Average of 10 microprobe analyses and Penfield tube data for H_2O in kalifersite.

Oxides	av.	range	standard
Na_2O	1.98	1.43–2.39	NaCl
K_2O	7.71	7.01–8.08	KBr
MgO	1.21	0.90–1.64	MgO
MnO	2.38	1.69–3.70	Mn
Fe_2O_3	17.96	16.66–20.23	hematite
SiO_2	55.39	53.16–57.73	SiO_2
CaO	0.35	0–1.02	wollastonite
H_2O	13.42	–	–
total	100.40		

Experimental

Occurrence and physical properties

Kalifersite occurs in a drill core (202 m depth) of a hydrothermally altered pegmatite in the urtite series (Khibina massif, Mt. Kukisvumchorr, Kola Peninsula, Russia); it is in close association (even at submicroscopic level) with aegirine, fenaksite, pectolite and an unidentified light-green mineral. Other associated minerals are: potassium feldspar, sodalite, nepheline, aenigmatite, lomonosoite, lamprophyllite, scherbakovite, loparite, natisite, paranatisite and sphalerite. Kalifersite formed by crystallization from residual peralkaline liquids during the hydrothermal stage of the pegmatitic process. It is fibrous [001] and forms millimetric bundles (up to 5 mm long) and aggregates (up 1 cm) within cavities of the rock.

Kalifersite is pink-brownish and translucent with white streak and silky to earthy lustre; fluorescence is absent with UV 240–400 nm (in air); [001] fibrous parting; $H = 2$ (Mohs); {100} and {010} good cleavages; brittle, fibrous fracture. The measured and calculated densities are 2.37(2) (heavy liquids) and 2.28 g/cm³ (see below), respectively. Biaxal (+); at 589 nm $\alpha = 1.523(2)$, $\beta = 1.525(2)$, $\gamma = 1.550(2)$, *2V(meas)* = 30(2)°, *2V(calc)* = 32°; dispersion is not discernible; optically pseudo-orthorhombic, presumably because the single fibres are disordered around [001]; $X \approx$ **a**, $Y \approx$ **b**, $Z \approx$ **c**, *O.P. (010)*; the pleochorism is medium with Z = yellow, Y and X slightly pink. The compatibility according to Mandarino (1981) is 0.002 (superior).

Chemical data

DTA shows an endothermic effect at 150°C connected with dehydration; TGA gives a weight loss

of 13.1 % at 1000°C. The infrared spectrum shows bands at 3435 (strong), 1655 (strong), 1015 (strong), 785, 730, 645, 540 (strong), 510, 450 (strong) (cm^{-1}).

The results of 10 analyses by electron microprobe on a SEM (Cambridge) equipped with EDS 860-Link System (15 kV, 500 pA) are reported in Table 1; $Fe_{tot} = Fe^{3+}$ has been proved by wet analyses. The value of H_2O shown in Table 1 has been obtained by Penfield tube and well agrees with TGA value; CO_3 was not detected by infrared spectroscopy. Kalifersite is readily decomposed by 10% HCl and HNO_3 at room temperature. On the basis of $O = 68$ (*cf.* below) the following empirical formula is obtained from the data in Table 1:

$(K_{3.58}Na_{1.40})_{\Sigma 4.98}[(Fe^{3+})_{4.92}Mn_{0.73}Mg_{0.66}Ca_{0.14})]_{\Sigma 6.45}$
$[Si_{20.16}O_{50}][(OH)_{3.44}(H_2O)_{14.56}]_{\Sigma 18}$. It leads to *MW* = 2195.67 and *D(calc)* = 2.28 g/cm³ for $Z = 1$ in all cell with $V = 1600$ Å³ (see below). A simplified formula $(K,Na)_5(Fe^{3+})_7[Si_{20}O_{50}](OH)_6 \cdot 12H_2O$ can be assigned to kalifersite; for $K = 4$ and $Na = 1$ it requires $K_2O = 8.37$, $Na_2O = 1.38$, $Fe_2O_3 = 24.84$, $SiO_2 = 53.40$, $H_2O = 12.01$, $MW = 2250.3$, *D(calc)* = 2.33 g/cm³. Discrepancies with *D(meas)* = 2.37(2) g/cm³ can be attributed to variable chemical composition as discussed below.

Crystallography

Due to the [001] fibrous morphology, no single crystals suitable for X-ray diffraction have been found: apparent "individuals" are actually bundles with disorder around the elongation direction; single crystals are (100) lamellae [001] elongated and few hundred Å wide in the [010] direction.

Diffraction data used to decipher crystallographic and structural features of kalifersite are X-
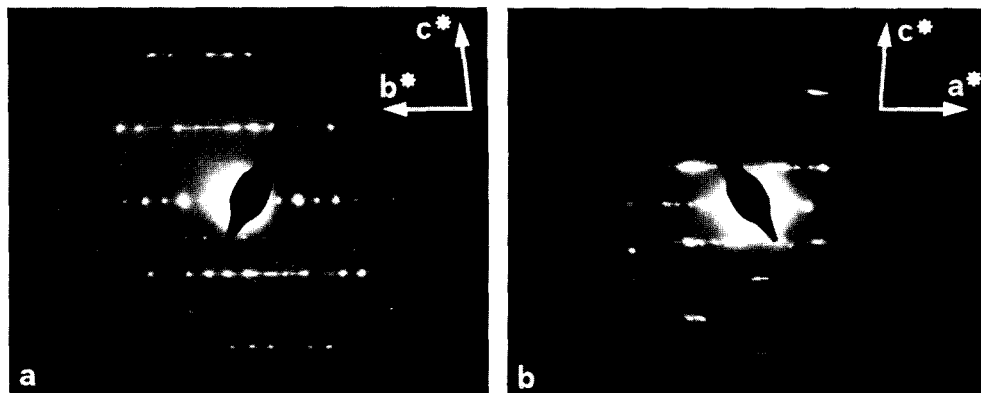
Fig. 1. SAED pictures of kalifersite along [100] (a) and [010] (b).

ray powder patterns (diffractometer, Co$K\alpha$ and Cu$K\alpha$; Gandolfi and Guinier cameras, Cu$K\alpha$) together with $0kl$ and $h0l$ selected area electron diffractions (SAED); SEM and TEM images have been observed too. The SAED patterns (Fig. 1; CM12 Philips electron microscope) show triclinic symmetry and structural disorder; doubling of the b axis is suggested by weak reflections with $k = 2n + 1$ which tend to be masked by diffuse streaks along b^*. This doubling is confirmed by the successful indexing of the powder pattern (Table 2), leading to a least-squares refined cell (unit weights) with $a = 14.86(4)$, $b = 20.54(4)$, $c = 5.29(2)$ Å, $\alpha = 95.6(3)$, $\beta = 92.3(3)$, $\gamma = 94.4(3)°$, and by the structural model (see below). In particular, the doublet at 12.36 + 11.60 Å can be indexed as $\bar{1}10$ and 110, respectively, only on the basis of the shown cell. The values of the diffraction intensities calculated (SHELXTL package; Sheldrick, 1990) from the structural model (Table 3) have been taken into account in indexing the X-ray powder diffraction pattern; in agreement with $0kl$ SAED, only 050 shows a significant intensity among $0kl$ reflections with $k = 2n + 1$ (Table 3). The powder diffraction data given in Table 2 have been collected by a Siemens-D5000 diffractometer and processed by the annexed DIFFRAC AT package: graphite-monochromatized CuKα radiation; 0.02° steps of 2θ; 30s counting for each step.

Structural model

Preamble

The experimental data of kalifersite have been interpreted by comparison with sepiolite {ideally

$Mg_8[Si_{12}O_{30}](OH)_4 \cdot 12H_2O$; $a = 13.40$, $b = 26.80$, $c = 5.28$ Å, s. g. $Pncn$, $Z = 2$ (Brauner & Preisinger, 1956)} and palygorskite {ideally $Mg_5[Si_8O_{20}](OH)_2 \cdot 8H_2O$; two polytypes are known (Artioli & Galli, 1994) with $a = 13.27$, $b = 17.868$, $c = 5.279$ Å, $\beta = 107.38°$, s. g., $C2/m$, $Z = 2$ and $a = 12.763$, $b = 17.842$, $c = 5.241$ Å, s. g. $Pbmn$, $Z = 2$}. In particular, the following data are of interest:

(i) Kalifersite, sepiolite and palygorskite have close values of a and c parameters, the latter corresponds to the fibrous direction of these silicates and to the periodicity of a pyroxene chain.

(ii) The b value of kalifersite is intermediate between that of palygorskite and sepiolite.

(iii) The structures of sepiolite and palygorskite are based on a framework of [001] TOT ribbons (triple-chain I beam) which are chess-board arranged and intercalated with channels. In the b direction, the $(TOT)_S$ ribbon of sepiolite is one chain wider than that, $(TOT)_P$, of palygorskite; this feature requires for sepiolite a b value about 9 Å longer than that of palygorskite, i.e. about 4.5 Å per T chain.

(iv) Jones & Galan (1988) have summarized results which show that both palygorskite (see also Artioli & Galli, 1994) and sepiolite can occur as different polymorphs (or polytypes) differing very little with respect to a basic structure, the main differences being changes in symmetry. Besides, these minerals can contain both trivalent cations, in their octahedral strips, and extra cations in their channels, balancing the charges through octahedral vacancies and tetrahedral substitutions.

Table 2. Observed (I_O and d_O) and calculated (I_c and d_c) intensities (relative scale) and interplanar spacings (Å) with the corresponding indexes (hkl) for the powder diffraction pattern of kalifersite with CuKα radiation. The most intense lines of aegirine (A), fenaksite (F) and pectolite (P), which are present as impurities, are shown; b broad line; *not used in the cell refinement.

I_O	I_c	d_O	d_c	hkl
100	100	12.36	12.46	$\bar{1}10^*$
40	90	11.60	11.54	110
14	8	10.21	10.19	020
3	4	8.77	8.73	$\bar{1}20$
4	3	8.03	8.09	120
6	1	7.68 Pb	7.40	200^*
5	3	6.34 A	6.37 6.23	$\bar{1}30\ \bar{2}20^*$
2	2	5.22	5.22	$\bar{2}30$
4	2	5.10 b	5.03 4.97 4.97	$\bar{1}01\ 011\ \bar{1}\bar{1}1$
2	3	4.79	4.88 4.88 4.81	$\bar{1}\bar{1}1\ 101\ 230$
2	2	4.65	4.71 4.59	$310\ \bar{3}20$
2	2	4.505	4.492	021
9	2	4.397 A	4.393	$\bar{1}21$
2	2	4.290	4.305 4.257	$320\ \bar{2}11$
5	11	4.162	4.212 4.209 4.184	$\bar{1}31\ 121\ \bar{1}\bar{3}1$
4	10	4.075	4.083 4.075	$\bar{2}\bar{2}1\ 050$
2	3	3.984	4.045 3.968	$240^*\ 031$
5	18	3.818 b	3.859 3.748 3.700 3.697	$0\bar{4}1\ \bar{2}\bar{3}1\ 400^*\ \bar{3}40^*$
3	3	3.553	3.589 3.515 3.487	$410\ 301\ 041^*$
37	6	3.411 Fb	3.408 3.400 3.393	$340\ 060\ 311$
15	2	3.281 Pb	3.280 3.266	$\bar{1}\bar{5}1\ \bar{2}41$
4	3	3.182	3.227 3.201	$\bar{3}31^*\ 321$
4	1	3.130	3.143 3.097	$430\ \bar{4}01^*$
5	2	3.075 FP	3.065 3.065	$\bar{4}11\ \bar{1}51$
5	5	2.980 A	2.994 2.973 2.972 2.970 2.964	$0\bar{6}1\ 331\ \bar{3}41\ \bar{4}21\ \bar{5}10$
12	6	2.896 AFP	2.910 2.896	$\bar{1}\bar{6}1\ 510$
4	2	2.827 b	2.843 2.827	$4\bar{3}1^*\ \bar{4}31$
1	1	2.750	2.754 2.748	$421\ \bar{3}\bar{5}1$
2	4	2.738	2.737 2.720	$341\ \bar{3}51^*$
2	4	2.631	2.639	$\bar{2}61$
3	4	2.575	2.584 2.568	$1\bar{1}2\ 102$
4	1	2.544	2.524	$5\bar{2}1$
2	2	2.503	2.511 2.485	$\bar{3}\bar{6}1\ \bar{3}61$
4	16	2.465 F	2.467 2.467 2.459	$\bar{2}\bar{7}1\ 600\ 2\bar{1}2$
3	2	2.389 b	2.389 2.379 2.368	$0\bar{8}1\ 4\bar{6}1\ \bar{3}02^*$
2	2	2.357	2.354 2.338 2.333	$620\ \bar{1}\bar{8}1\ \bar{3}\bar{2}2^*$
4	7	2.290	2.298 2.275	$\bar{4}61\ \bar{3}02^*$
3	6	2.246	2.273 2.247	$\bar{3}71\ \bar{1}42$
5	4	2.196	2.215 2.211 2.191 2.190 2.189	$4\bar{7}1^*\ 190\ \bar{5}\bar{5}1\ \bar{6}50\ \bar{4}\bar{1}2$
4	3	2.161	2.169 2.155 2.154	$\bar{2}81\ 1\bar{9}1\ 181$
2	3	2.122	2.115 2.113 2.112	$371\ 4\bar{1}2\ \bar{4}\bar{7}1$
3	3	2.109	2.108 2.106	$461\ \bar{3}\bar{8}1$
2	2	2.035	2.060 2.043 2.042	$\bar{5}\bar{6}1\ 551\ \bar{2}\bar{9}1$
5	3	2.017 b	2.020 2.014 2.011 2.009	$631\ \bar{5}02\ \bar{7}40\ \bar{5}\bar{1}2$
2	1	1.992	1.985 1.983 1.972	$\bar{5}22\ \bar{2}91\ \bar{7}21^*$
5	1	1.730 P	1.766	$\bar{6}\bar{7}1^*$
3	2	1.611	1.610 1.607	$702\ 3\bar{4}3$
3	1	1.592	1.601 1.600	$\bar{7}81\ \bar{8}61$
2	2	1.560	1.565 1.565 1.556	$1\bar{7}3\ \bar{1}\bar{7}3\ 871$

(v) Martin-Vivaldi & Linares-Gonzales (1962) have interpreted diffraction patterns intermediate between those of palygorskite and sepiolite on the basis of random intergrowth of *(TOT)$_S$* and *(TOT)$_P$* ribbons.

The model

Taking into account the above features and following a procedure based on polysomatism theory, which has already been used in similar cases

(Ferraris et al., 1996b; Ferraris, 1997), the structural model illustrated in Fig. 2 has been deduced for kalifersite. Main characteristics of this model are (i) a chess-board arrangement of $(TOT)_P$ and $(TOT)_S$ [001] ribbons and (ii) filling of the [001] channels with alkalis and water molecules. The six independent water molecules pfu (OW in Table 3) are coordinated by the three independent alkali atoms only. All the alkalis have six-fold coordination; however, while $K3$ is bonded to H_2O only, $K1$ and $K2$ coordinate also two oxygens each (in the order: $O1$ and $O6$, $O3$ and $O13$; Table 3). The K-octahedra are arranged according to two different [001] strips; each one is either two or three rows wide and bridges, along [010] and in the order, the Fe-octahedral strips of either two $(TOT)_S$ or two $(TOT)_P$ ribbons. Consequently, two types of bidimensional mixed (100) octahedral sheets are formed, as further discussed below. This model is able to explain the observed features of kalifersite:

1. A b value smaller than that expected (about 22.5 Å) for a width of five T chains corresponds to a stretching along a of the channels which, in contrast to sepiolite and palygorskite, are now completely filled by large cations.

2. Agreement between observed and calculated diffraction intensities of the powder pattern (Table 2) might look not very good; it must, however, be taken into account that the quality of the pattern is affected by low crystallinity, structural disorder in the chess-board arrangement (cf. streaks in SAED both along a^* and b^*; Fig. 1), impurities (Table 2) at submicroscopic level and preferred orientation. Such data, together with the complexity of the low symmetry structure, render unfeasible a Rietveld refinement according to the authors experience (Ferraris et al., 1995; Pavese et al., 1997). The coordinates of the structural model reported in Table 3 have been optimized (R = 0.06) by a least-squares procedure according to the program DLS76 (Baerlocher et al., 1978).

3. The [001] elongation of the fibres is due to the structural TOT ribbons, while the (100) lamellar morphology of the single-crystals is connected with the (100) structural layers. The {100} and {010} good cleavage are clearly related to the features of the (001) cross-sections of the TOT ribbons.

4. Chemical composition, including an easy (150°C in DTA) loss of water which is loosely bonded to K in the channels.

Table 3. Calculated fractional coordinates for the atomic positions in kalifersite (DLS refinement) OW represents the oxygen of the water molecules.

| atom	x	y	z
Fe1	0	0	0
Fe2	0.000	0.077	0.507
Fe3	0.508	0.318	0.175
Fe4	0.506	0.389	0.702
Fe5	0.501	0.463	0.234
Si1	0.181	0.068	0.834
Si2	0.176	0.122	0.334
Si3	0.319	0.306	0.816
Si4	0.315	0.448	0.876
Si5	0.319	0.235	0.274
Si6	0.311	0.525	0.415
Si7	0.300	0.670	0.472
Si8	0.293	0.742	-0.003
Si9	0.191	0.932	0.796
Si10	0.192	0.866	0.268
K1	0.519	0.108	0.069
K2	0.010	0.274	-0.004
K3	0	1/2	1/2
O1	0.074	0.078	0.843
O2	0.080	0.004	0.340
O3	0.075	0.147	0.283
O4	0.428	0.312	0.833
O5	0.424	0.456	0.889
O6	0.427	0.234	0.253
O7	0.423	0.383	0.361
O8	0.420	0.531	0.424
O9	0.413	0.602	-0.048
O10	0.411	0.677	0.483
O11	0.403	0.748	0.982
O12	0.082	0.932	0.816
O13	0.081	0.858	0.274
O14	0.208	0.001	0.673
O15	0.207	0.121	0.635
O16	0.195	0.059	0.136
O17	0.260	0.165	0.225
O18	0.274	0.273	0.050
O19	0.285	0.266	0.546
O20	0.270	0.373	0.839
O21	0.279	0.474	0.615
O22	0.287	0.483	0.144
O23	0.265	0.593	0.480
O24	0.259	0.716	0.704
O25	0.267	0.686	0.189
O26	0.245	0.805	0.132
O27	0.216	0.926	0.095
O28	0.219	0.877	0.574
OW29	0.351	0.013	0.999
OW30	0.613	0.107	0.579
OW31	0.130	0.414	0.179
OW32	0.891	0.381	0.755
OW33	0.060	0.293	0.500
OW34	0.147	0.523	0.902
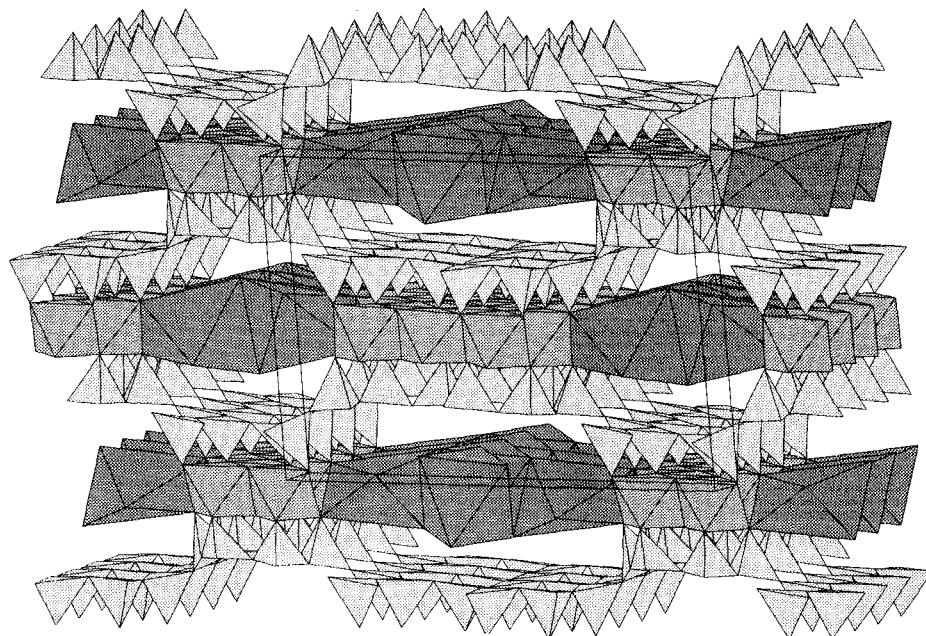
Fig. 2. Perspective view along [001] of the crystal structure of kalifersite. Alkali octahedra are dark dotted.

Discussion

Crystal chemistry

According to the structural model (Fig. 2; Table 3), the ideal crystallochemical formula of kalifersite is $A_5Y_9[Si_{20}O_{50}](OH)_6 \cdot mH_2O$ (Z = 1); $m \geq 12$ to provide at least six-fold coordination to the large cations A = (K, Na) which occur in the [001] structural channels of the sepiolite/palygorskite framework. In the analyzed samples of kalifersite (Table 1), m is close to 12, but a different (higher) quantity of H_2O can be expected in freshly collected samples because it is loosely bonded to the structure. The Y cation of the octahedral strips is in mainly Fe^{3+} (plus Mn, Mg and Ca in order; Table 1), with an average of 6.5 apfu, i.e. lower than the nine available Y sites. A variable occupancy of these sites occurs also in palygorskite and sepiolite, where Y is mainly bivalent, and is related to the oxidation state of Y and the quantity and type of A. In kalifersite the large amount of Fe^{3+} cannot allow full occupancy which, in fact, is close to 2/3 of the available Y sites. The nature and quantity of Y cations is also related to the number of OH groups which, however, cannot exceed 6 pfu, i.e. the number of the framework oxygens which are linked to M only ($O2$, $O7$ and

$O9$ in Table 3). The other oxygens are bonded to Si only (from $O14$ to $O28$ in Table 3) or to one Si plus Y and A cations.

The above discussion shows that a variable chemical composition and, consequently, variable properties can be expected for kalifersite, as reported by Khomyakov (1995), where data for this mineral are given under code $M27$. Further, minerals intergrown with kalifersite at submicroscopic level (see above) can contribute to bulk wet chemical analyses, as that given by Khomyakov (1995), and increase the value of $D(meas)$, in comparison with $D(calc)$. The latter effect may be further enhanced by the mobility of water.

Polysomatic interpretation

Palygorskite and sepiolite can contain octahedral Y^{3+} cations, besides Mg (mainly), and some A^{n+} cations are statistically distributed together with H_2O in the structural [100] channels. Therefore, the general formulae for these two minerals can be written in the following way (modified from Jones & Galan, 1988; tetrahedral substitutions ignored; channel content enclosed in brace):
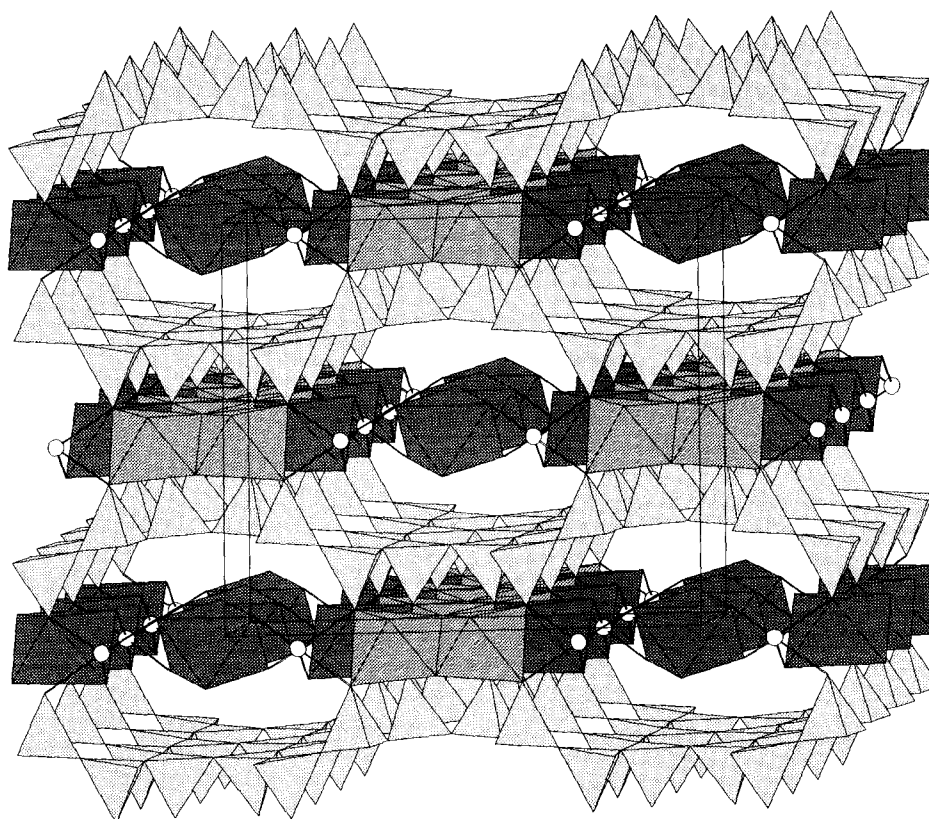
$P = [(Y^{2+})_{5-y'-z'}(Y^{3+})_{y'}\square_{z'}][Si_8O_{20}](OH)_2$
$\{(A^{n+})_{(2z'-y')/n}\ m'H_2O\}$ (palygorskite module);
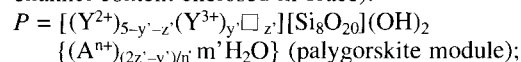
Fig. 3. Perspective view along [001] of the crystal structure of raite. Alkali octahedra are dark dotted; open circles represent the partially occupied Ti positions.

$S = [(Y^{2+})_{8-y-z}(Y^{3+})_y\square_z][Si_{12}O_{30}](OH)_4\{(A^{n+})_{(2z-y)/n}$
$\cdot mH_2O\}$ (sepiolite module).

Kalifersite $K_5(Fe^{3+})_7[Si_{20}O_{50}](OH)_6\cdot 12H_2O$ can be considered the P_lS_l member (with $y + y' = 7$, $z + z' = 6$ and $m + m' = 12$) of a polysomatic series P_pS_s with general formula

$\{[(Y^{2+})_{5-y'-z}(Y^{3+})_{y'}\square_{z'}][Si_8O_{20}](OH)_2$
$\{(A^{n+})_{(2z'-y')/n}\cdot m'H_2O\}\}_p$
$\{[Y^{2+})_{8-y-z}(Y^{3+})_y\square_z][Si_{12}O_{30}](OH)_4$
$\{(A^{n+})_{2z-y)/n}\cdot mH_2O\}\}_s$.
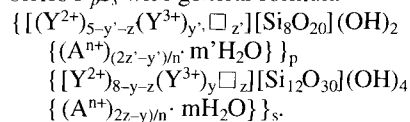
This series shall be called *palysepiole polysomatic series, palysepiole* being an acronym constructed from *paly*gorskite and *sepio*lite; *palysepioles* shall be the members of the series.

The series P_pS_s and, in particular, kalifersite can be compared with mica and, more generally, with biopyriboles. Zoltai (1981) defined *DiC* and *TriC* as *TOT* basic layer modules corresponding, respectively, to one-chain wide (010) slabs of

dioctahedral *(Di)* and trioctahedral *(Tri)* micas with a total height *t* of about 10 Å. *C* stands for interlayer cation and is omitted for pyroxenes and amphiboles with empty *A* site; *1/2TriC* has been used to describe intermediate tri- and di-octaheral layers, as occurring in palygorskite and sepiolite. The vertical shifts ([100] direction in palysepioles) between basic modules can be *nt* (*n = 0, 1/2, 3/4*); *n = 0* corresponds to the major layer silicates, like micas; in pyroxenes and amphiboles *n = 1/2*, while *n = 3/4* describes the shift between ribbons in palygorskite, sepiolite and, now, kalifersite. According to Zoltai's symbolism, and taking into account that some interlayer cations can occur, palygorskite and sepilote represent the members *1/2TriC-0-1/2TriC-3/4* and *1/2TriC-0-1/2TriC-0-1/2TriC-3/4* of the biopyribole series (or group); the new member kalifersite (ideally only Y^{3+} in the octahedral sheet) corresponds to *DiC-0-DiC-3/4-DiC-0-DiC-0-DiC-3/4*.

The interpretation of kalifersite as a member of the P_pS_s polysomatic series and the connection of this series with biopyriboles suggest that defects based on the polysomatic modules can be source of variable composition and diffraction streaks because of stacking faults both in [100] and [010] directions.

Related minerals

Falcondoite (a = 13.5, b = 29.9, c = 5.24 Å; Springer, 1976) and loughlinite (Fahey et al., 1960) differ from sepiolite just for the presence of Ni and Na, respectively. Yofortierite (Perrault et al., 1975) and tuperssuatsiaite (a = 13.92, b = 17.73, c = 5.30 Å, β = 104.78°; von Knorring et al., 1992) are, in the order, Mn and Fe equivalent of palygorskite. Even if the crystal structures of these four minerals have not been explicitly determined, their chemical data and lattice dimensions support the hypothesis of isostructurality with sepiolite or palygorskite.

Besides the case of kalifersite, the flexibility in building crystal structures offered by the structural modules of palygorskite and sepiolite comes out particularly evident from the recent crystal structure determinations of intersilite (Egorov-Tismenko et al., 1996; Yamnova et al., 1996) {(Na,K)Mn(Ti,Nb)Na$_5$(O,OH)(OH)$_2$[Si$_{10}$O$_{23}$(O,OH)$_2$]· 4H$_2$O; a = 13.033, b = 18.717, c = 12.264 Å, β = 99.62°, s. g. $I2/m$, Z = 4} and raite (Pluth et al., 1997) {Na$_3$Mn$_3$Ti$_{0.25}$[Si$_8$O$_{20}$](OH)$_2$·10H$_2$O; a = 15.1, b = 17.6, c = 5.290 Å, β = 100.5°; s. g. $C2/m$, Z = 2; Fig. 3}. In intersilite, sepiolite-like ribbons partially overlap along [010] thanks to tetrahedral inversion within the same ribbon. The overlap reduces the length of b to 18.7 Å , as compared with 26.8 Å in sepiolite, and the supplementary tetrahedral inversion brings the periodicity along c to 2.5 times (5 tetrahedra = 12.3 Å) that of the pyroxene-like tetrahedral chain.

Bridges between layer silicates

The presence of a continuous two-dimensional tetrahedral sheet is a characteristic of phyllosilicates. In the stricto sensu phyllosilicates, this tetrahedral sheet is associated with a continuous octahedral sheet and only weak forces connect 1:1 (TO) or 2:1 (TOT) layers. Due to the misfit between tetrahedral and octahedral sheets, cases showing either (i) tetrahedral inversions [without (e.g., antigorite) or with (e.g., sepiolite and palygorskite) interruption of the octahedral sheet] or (ii) interruption of the tetrahedral sheet (e.g., carlosturanite; Mellini et al., 1985) are known (Guggenheim & Eggleton, 1988). Because of the presence of strong bonds between the "layers", cases (i) (inverted-layer silicates) are usually considered only lato sensu phyllosilicates (layer silicates).

The mentioned structure of raite (Fig. 3) consists of a palygorskite-like framework, where each [001] channel is partially filled with a row of isolated Na-octahedra; this row, in its turn, is loosely linked to octahedra of two $(TOT)_p$ ribbons through Ti-octahedra which have only 1/8 occupany. Both raite (Fig. 3) and kalifersite (Fig. 2) can be considered examples of lato sensu 2:1 layer structures, where a (quasi, in raite) continuous octahedral sheet is sandwiched between two inverted tetrahedral sheets. In contrast with the true 2:1 layer structures, in raite and kalifersite the tetrahedral sheet is attached to a part only of octahedra, i.e. mainly to those which do not contain alkalis. That reflects the difficulty of fitting large alkaline octahedra within the compass of the tetrahedral sheet, even for strips which are only few rows wide.

Within a sepiolite/palygorskite (010) slab one ribbon wide, kalifersite (and approximately raite) show, along [100], a chlorite-like topology, i.e. a $TOTO'TOT$ sequence; O' represents the alkali strip. On this basis and Zoltai's (1981) proposal, a further modular connection is established between the P_pS_s polysomatic series described in this paper (palysepiole series), the mixed-layer silicates and the biopyriboles.

Conclusions

The application of the concepts of modular crystallography, particularly polysomatic theory, has allowed to obtain a structural model which is able to explain the major characteristics of the new fibrous silicate kalifersite and to connect them with those of other lato sensu layer silicates.

It can be emphysized that, as already proved [e.g., with nafertisite (Ferraris et al., 1996b)], the use in a broader sense of the basic concepts established for the polysomatic series (Thompson, 1978) shows to be very fertile. Particular reference is made to the utilization of the topologic characteristics of the building modules disregarding, if the case, the real chemical composition.

Actually, there are now several examples (Ferraris, 1997; Merlino, 1997) proving that the concept (and the basic definition) of polysomatism can be profitable applied, at least in silicates, just considering essential features, like crystallochemical data and geometry of the lattice. This information alone can disclose the presence, in the studied material, of modules whose topology is already known.

References

Artioli, G. & Galli, E. (1994): The crystal structures of orthorhombic and monoclinic palygorskite. *Mat. Sci. Forum*, **166–169**, 647–642.

Baerlocher, Ch., Hepp, A., Meier, W.M. (1978): DLS-76 Manual. A program for the simulation of crystal structures by geometric refinement. ETH, Zürich.

Brauner, K. & Preisinger, A. (1956): Struktur und Entstehung des Sepioliths. *Tscherm. Miner. Petrogr. Mitt.*, **6**, 120–140.

Egorov-Tismenko, Yu.K. & Sokolova, E.V. (1990): Structural mineralogy of the homologic series seidozerite-nacaphite. *Mineral. Zhurn.*, **12**, 40–49 (in Russian).

Egorov-Tismenko, Yu.K., Yamnova, N.A., Khomyakov, A.P. (1996): A new representative of a series of chain-sheet silicates with inverted tetrahedral fragments. *Crystallogr. Rev.*, **41**, 784–788.

Fahey, J.J., Ross, M., Axelrod, J.M. (1960): Loughlinite, a new hydrous sodium magnesium silicate. *Amer. Mineral.*, **45**, 270–281.

Ferraris, G. (1997): Polysomatism as a tool for correlating properties and structure. *in* Merlino, S. (ed.): Modular aspects in minerals. *EMU Notes Mineral.*, **1**, 275–295.

Ferraris, G., Ivaldi, G., Khomyakov, A.P. (1995): Altisite $Na_3K_6Ti_2[Al_2Si_8O_{26}]$ Cl_3 a new hyperalkaline aluminosilicate from Kola Peninsula (Russia) related to lemoynite: crystal structure and thermal evolution. *Eur. J. Mineral.*, **7** 537–546.

Ferraris, G., Ivaldi, G., Khomyakov, A.P., Soboleva, S.V., Belluso, E. (1996a): Polysomatism, a key to characterize the new silicate kalifersite from Kola Peninsula (Russia). *Acta Miner.-Petrogr. Suppl., Hungary*, **37**, 36.

Ferraris, G., Ivaldi, G., Khomyakov, A.P., Soboleva, S.V., Belluso, E., Pavese, A. (1996b): Nafertisite, a layer titanosilicate member of a polysomatic series including mica. *Eur. J. Mineral.*, **8**, 241–249.

Ferraris, G., Khomyakov, A.P., Belluso, E., Soboleva, S.V. (1997): Polysomatic relationships in some titanosilicates occurring in the hyperagpaitic alkaline rocks of the Kola Peninsula, Russia. Proc. 30th Int. Geol. Congr., Vol. **16**, "Mineralogy", 17–27.

Ferraris, G., Pavese, A., Soboleva, S.V. (1995): Tungusite: new data, relationship with gyrolite and structural model. *Min. Mag.*, **59**, 535–543.

Guggenheim, S. & Eggleton, R.A. (1988): Crystal chemistry, classification, and identification of modulated layer silicates. *in* Bailey, S.W. (ed.): Hydrous phyllosilicates. *MSA Rev. Mineral.*, **19**, 675–718.

Jones, B.F. & Galan, E. (1988): Sepiolite and palygorskite. *in* Bailey, S.W. (ed.): Hydrous phyllosilicates. *MSA Rev. Mineral.*, **19**, 632–674.

Khomyakov, A.P. (1995): Mineralogy of hyperagpaitic alkaline rocks. Clarendon Press, Oxford.

Liebau, F.: (1985): Structural chemistry of silicates. Springer-Verlag, Berlin.

Lima-de-Faria, J. (1994): Structural Mineralogy – An Introduction. Kluwer Acad. Publ., Dordrecht.

Mandarino, J.A. (1981): The Gladstone-Dale relationship: Part IV. The compatibility concept and its application. *Canad. Mineral.*, **19**, 441–445.

Martin-Vivaldi, J.L. & Linares-Gonzales, J. (1962): A random intergrowth of sepiolite and attapulgite. *Clay & Clays Min.*, **9**, 592–602.

Mellini, M., Ferraris, G., Compagnoni, R. (1985): Carlosturanite: HRTEM evidence of a polysomatic series including serpentine. *Amer. Mineral.*, **70**, 773–781.

Merlino, S. (ed.) (1997): Modular aspects in minerals. *EMU Notes Mineral.*, **1**. Budapest, Eötvös Univ. Press.

Pavese, A., Ferraris, G., Prencipe, M., Ibberson, R. (1997): Cation-site ordering in phengite-3T from the Dora-Maira massif (western Alps): a variable-temperature neutron powder-diffraction study. *Eur. J. Mineral.*, **9**, 1183–1190.

Perrault, G., Harvey, Y., Pertsowsky, R. (1975): La yofortierite, un nouveau silicate hydraté de manganèse de St.-Hilaire, P.Q. *Canad. Mineral.*, **13**, 68–74.

Pluth, J.J., Smith, J.V., Pushcharovsky, D.Yu., Semenov, E.I., Bram, A., Reikel, Ch., Weber, H.-P. Broach, H.-P. (1997): Third-generation synchrotron X-ray diffraction of six-micrometer crystal of raite, $Na_3Mn_3Ti_{0.25}Si_8O_{20}(OH)_2 \cdot 10H_2O$, opens up new chemistry and physics of low-temperature minerals. *Proc. Nat. Acad. Sci.*, **94**, 12263–12267.

Sheldrick, G.M. (1990): SHELXTL PC, An integrated system for solving, refining and displaying crystal structures from diffraction data (Revision 4.1). Reference Manual, SIEMENS, 1–296.

Springer, G. (1976): Falcondoite, nickel analogue of sepiolite. *Canad. Mineral.*, **14**, 407–409.

Thompson, J.B., Jr. (1978): Biopyriboles and polysomatic series. *Amer. Mineral.*, **63**, 239–249.

von Knorring, O., Petersen, O.V., Karup-Moller, S., Leonardsen, E.S., Condliffe, E. (1992): Tuperssuatsiaite, from Aris phonolite, Windhoek, Namibia. *N. Jb. Miner. Mh.*, **1992**, 145–152.

Yamnova, N.A., Egorov-Tismenko, Yu.K., Khomyakov, A.P. (1996): Crystal structure of a new natural (Na,Mn,Ti)-phyllosilicate. *Crystallogr. Rev.*, **42**, 239–244.

Zoltai, T. (1981): Amphibole asbestos mineralogy. *in* Veblen, D.R. (ed.): Amphiboles and other hydrous pyriboles. *MSA Rev. Mineral.*, **9a**, 237–278.